http://dx.doi.org/10.21577/0103-5053.20190115

J. Braz. Chem. Soc., Vol. 30, No. 10, 2210-2218, 2019
Printed in Brazil - ©2019 Sociedade Brasileira de Química

Article

Facile One-Step Electrodeposition Fabrication of Amorphous MoS_2 Catalysts in Titanium for Hydrogen Evolution Reaction

Marina Medina,[a] *Patricia G. Corradini*[a] *and Lucia H. Mascaro*[*,a]

[a]*Departamento de Química, Universidade Federal de São Carlos, Rod. Washington Luís, km 235, 13565-905 São Carlos-SP, Brazil*

Hydrogen is seen as a future energy carrier that will assist the global energy fuel demand. However, it is still necessary to study efficient and inexpensive catalysts that can be used on a large scale to make this technology practical. In this paper the electrodeposition of molybdenum disulfide (MoS_2) film on titanium (Ti) substrate was performed by cyclic voltammetry and the film was evaluated for hydrogen evolution reaction (HER). The deposition optimized conditions was 25 cycles and 4 mmol L^{-1} $(NH_4)_2[MoS_4]$ in 0.1 mol L^{-1} $NaClO_4$ solution. The film was characterized from X-ray diffraction (XRD), scanning electron microscopy (SEM), energy dispersive X-ray spectroscopy (EDX) and they showed an amorphous structure and high catalytic activity for HER. The Tafel slope was 85 mV dec^{-1} and overpotential at −10 mA cm^{-2} was −139 mV showing that Ti substrate compared with fluorine-tin doped oxide (FTO) substrate favored the HER and electroactivity of MoS_2 films.

Keywords: molybdenum sulfide, titanium, hydrogen evolution reaction, electrodeposition, thin films

Introduction

In face of the global energy crisis and the environmental problems caused by the intense use of fossil fuels, there is need for development of alternative energy sources that are clean, renewable, and economically attractive.[1,2] In this sense, the use of hydrogen as an energy carrier is highlighted. One of its positive characteristics is its non-emission of greenhouse gases during the combustion process.[3,4] The most frequently used method to produce hydrogen currently is steam methane reforming, which uses high temperatures and produces CO_2. An interesting and viable alternative to obtaining hydrogen is the water splitting process,[5] which can be divided into the oxygen evolution reaction (OER) and the hydrogen evolution reaction (HER), as represented by equations 1 and 2.[6,7]

$$OER: H_2O \rightarrow {}^1/_2O_2 + 2H^+ + 2e^- \quad (1)$$

$$HER: 2H^+ + 2e^- \rightarrow H_2 \quad (2)$$

To increase the efficiency of obtaining hydrogen, the use of a highly active catalyst is necessary. A good electrocatalyst material for this system has to present high physical and chemical stability, low production cost, and be made by abundant elements for large-scale use.[8] The most efficient catalyst for HER in acidic medium is Pt.[9] However, factors such as high cost and scarcity make it a nonviable material. To overcome this limitation, several Pt-group metal-free (PGM-free) materials are being developed and applied as catalysts.[5,10-13] Indeed, catalysts that show reasonable current densities (j) at low overpotential (η) for HER remain an important research topic.[9,14]

One promising candidate for HER application is molybdenum disulfide (MoS_2).[7,15,16] MoS_2 is considered a stable, earth-abundant, nontoxic, and low cost material.[16] MoS_2 activity for HER is strongly influenced by its physical characteristics.[9,17] Some authors have suggested that this material is not an active HER catalyst in bulk form;[18] only nanostructures or amorphous MoS_2 are efficient.[14,19,20] These differences are justified in basal plane sites, which are catalytically inert and are thermodynamically favored in bulk. Amorphous and nanostructures present greater concentration of the edges layer sites, which show high activity for the HER.[7]

The preparation of MoS_2 amorphous materials is not easily synthesized, and may include solidification processes at milder temperatures.[9,20] The electrodeposition technique is an interesting method for obtaining amorphous material,

*e-mail: lmascaro@ufscar.br

and it can be operated rapidly in one-step fabrication in mild conditions, such as room pressure and temperature, and it can be incorporated into a full water-splitting device.[21] Some studies report MoS_x films growing in conductive substrates, such as fluorine-doped tin oxide (FTO), indium tin oxide (ITO), glassy carbon (GC) electrodes, and even in carbon paper or other structures of carbon nanotubes.[9,14,20,22,23] However, few papers have used this technique to study the deposition of MoS_2 in economical and chemical substrates that could be more easily employed on a large scale and under stable acidic conditions. This work shows a facile one-step electrodeposition fabrication of amorphous MoS_2 for HER, an inexpensive and chemically stable substrate: titanium. The same methodology was studied and optimized on FTO glass. The films were characterized using X-ray diffraction (XRD), scanning electron microscopy (SEM) and Raman spectroscopy, and we evaluated the catalytic activity of them toward the HER.

Experimental

Deposition of MoS_2 films

Ti foil (Impalla®, São Paulo, Brazil) and FTO (7 ohms sq^{-1}, Sigma-Aldrich®, Saint Louis, USA) with area equal to 1.5 cm^2 were used like working electrodes to perform the deposition of the MoS_2 films. The FTO was cleaned in ethanol, distilled water, and acetone. The Ti foil was first degreased in 10% (m/m) sodium hydroxide solution and then in 30% (m/m) hydrochloric acid solution at 100 °C for 1 h. Finally, the Ti foils were rinsed with distilled water and dried with N_2.

The electrochemical experiments were performed in an Autolab PGSTAT302N (Metrohm®). In all experiments, we used a three-electrode electrochemical system with a platinum plate (Impalla®, São Paulo, Brazil) and Ag/AgCl (saturated KCl) (Synth®, Diadema, Brazil) as the auxiliary and reference electrode, respectively. The electrolytes were thoroughly purged with nitrogen at room temperature. The electrolytic solutions were prepared from $(NH_4)_2[MoS_4]$ (Sigma-Aldrich®, Saint Louis, USA) and $NaClO_4$ (Merck®, Saint Louis, USA) as the supporting electrolytes. The films of MoS_2 were deposited on FTO by cyclic voltammetry (CV) at a scan rate of 50 mV s^{-1} between + 0.1 and −1.0 V. First, the precursor solution concentration and the number of applied cycles in the electrodeposition method were evaluated. The electrodes obtained in each experimental condition were nominated according to Table 1.

All obtained films were analyzed in a 0.5 mol L^{-1} H_2SO_4 solution for linear sweep voltammetry (LSV) at the scan rate of 1 mV s^{-1}. The optimized electrodeposition condition was considered for the film that presented lower η at −10 mA cm^{-2}, which is a reference value used because it represents a current density expected for a 12% efficient solar-to-hydrogen device.[7] The optimized condition was applied for the MoS_2 deposition on Ti foil. The deposited films were rinsed in distilled water, dried with N_2, and stored in the vacuum desiccator.

Table 1. Nomenclature of the molybdenum disulfide / fluorine-tin doped oxide (MoS_2/FTO) electrodes according to the parameters used in the electrodeposition

Film	Concentration of the precursor solution / (mmol L^{-1})	Number of applied cycles
1	2	13
2	2	25
3	2	50
4	4	13
5	4	25
6	4	50
7	6	13
8	6	25
9	6	50

Physical characterization

XRD measurements were evaluated by a Shimadzu XRD-6000 X-ray diffractometer (CuKα, λ = 1.54 Å). The scan rate was 2 min^{-1}. The film thickness and morphology were evaluated by dual-beam scanning electron microscopy (SEM) equipped with focused ion beam (FIB) observation equipment (FEI Vectra-IET). SEM integrates and makes it possible to realize a three-dimensional structure analysis. The composition of the films was studied by energy dispersive X-ray (EDX, FEI-XL30-FEG with Oxford Instruments-Link ISIS 300 detector). The morphology was characterized by SEM (FEI-Inspect F50 microscopy, Thermo Fisher Scientific®). The band gap value was analyzed by using UV visible diffuse reflectance spectroscopy (UV-Vis, Varian® Cary 5G). The Raman spectra were obtained with a micro Raman spectrometer SENTERRA (Bruker®). The laser had a wavelength of 532 nm and a power of 10 mW. The number of accumulations obtained for each spectrum was 3 with an integration time of 8 s and an approximate resolution of 3-5 cm^{-1}.

Catalytic activity experiments

Polarization curves were carried out in 1.0 mol L^{-1} H_2SO_4 (Sigma-Aldrich®, Saint Louis, USA) in distilled

water with a scan rate of 1 mV s^{-1} to analyze the catalytic activity of the prepared materials for HER. Potentials were referenced to a reversible hydrogen electrode (RHE) by adding a value of (0.197 + 0.059 pH) V, as reported in the literature.[24] The relationship between current and overpotential (η) at an electrical interface was given by the Butler-Volmer equation, and the high overpotential approximation will lead to the Tafel equation of the anodic and cathodic polarizations.[25] Therefore, for Tafel analysis, the logarithm of the current density of the resulting polarization curves was plotted *vs.* overpotential in a typical Tafel plot. With the resulting curve, we obtained the Tafel coefficient (b) and exchange current density (j_o) from the math analysis of the Tafel equation 3.[25]

$$\eta = b \log \frac{j}{jo} \quad (3)$$

Electrochemical impedance spectroscopy (EIS) measurements were also performed for the obtained films in FTO and Ti substrates, in H_2SO_4 (1.0 M) at −0.347 V (*vs.* Ag/AgCl). The frequency ranged from 10 kHz to 0.1 Hz and potential amplitude was of 5 mV.

Extended potential cycling was performed to evaluate the catalyst's durability. This experiment was performed by cycling the potential between −0.1 and −0.7 V *vs.* Ag/AgCl during 1000 cycles at 100 mV s^{-1} in 1.0 mol L^{-1} H_2SO_4.

Results and Discussion

Optimization of MoS_2 deposition

The method used for amorphous molybdenum sulfide deposition was cyclic voltammetry. First, we evaluated the precursor concentration and cycle numbers to optimize the deposition time. The best film would be that which presented lower η to HER as determined in −10 mA cm^{-2}. Figure 1 shows the cyclic voltammograms profile recorded for 4 mmol L^{-1} $(NH_4)_2[MoS_4]$ in 0.1 mol L^{-1} $NaClO_4$, pH 6.8 on the FTO substrate. In the first cycle the current values were small, but with the increasing number it was possible to observe a better definition of the anodic and cathodic processes, which were observed around −0.3 and −0.7 V, respectively. According to Morales-Guio and Hu,[20] the anodic process may be associated with the oxidation of the $[MoS_4]^{2-}$ species in MoS_3 according to the following reaction:

$$[MoS_4]^{2-} \rightarrow MoS_3 + \frac{1}{8}S_8 + 2e^- \quad (4)$$

On the other hand, during cathodic sweep, the specie $[MoS_4]^{2-}$ was reduced to MoS_2, and at the same time a brownish film started to form on the electrode, as described for equation 5.[20] The color change of film can be observed in the Figure 1a inset, which is a photo of film with 15 and 25 cycles.

$$[MoS_4]^{2-} + 2H_2O + 2e^- \rightarrow MoS_2 + 2HS^- + 2HO^- \quad (5)$$

The CV profiles in Figure 1a indicated a greater incorporation of the species involved in the deposition of the film during an increased number of cycles. The same voltammetric profile was observed for the nine electrodes produced in the FTO substrate. EDX spectroscopy was performed to evaluate the presence of S and Mo in the electrodeposited films. The results in Figure 1b show that the atomic ratio of Mo:S ranged between 1.8 and 2.2.

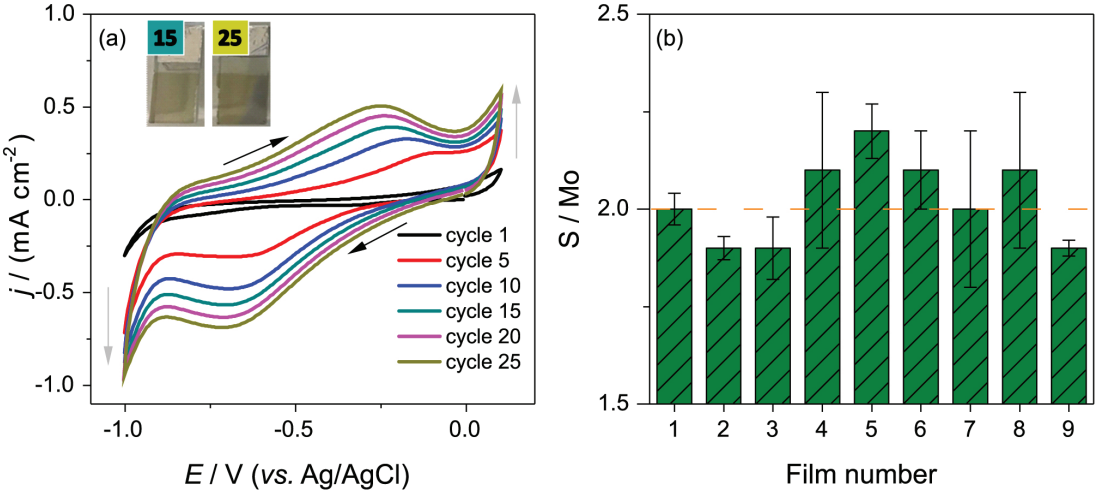

Figure 1. (a) Cyclic voltammograms of MoS_2 deposition on FTO substrate in 4 mmol L^{-1} $(NH_4)_2[MoS_4]$ in 0.1 mol L^{-1} $NaClO_4$ at a scan rate of 50 mV s^{-1}; (b) energy dispersive X-ray results of all obtained MoS_2 films.

Some studies in the literature[20,26,27] have reported that a mixture of amorphous MoS_3 and MoS_2 can be obtained by electrodeposition, usually noted as $MoS_{(2+x)}$. In our case, the ratio was approximately 2; therefore, we assumed that the specie deposited is MoS_2.

Figure 2a presents the polarization curves that were obtained using liner sweep voltammetry. In all curves, it is possible to observe that the cathodic current increased exponentially between −0.1 and −0.3 V due to HER. To compare the electrodes, Figure 2b shows the overpotential without iR compensation, determined at −10 mA cm^{-2} for all produced films, named as η_{10}. The η_{10} value ranged between −325 and −262 mV, which was a little higher than what has been reported in the literature, which is between −200 and −250 mV.[14,20] The differences values of η_{10} observed to nine electrodes are probably correlated to porosity change when electrodeposition conditions are altered. Merki *et al.*[14] studied the effect of cycle numbers in catalytic activity to HER and correlated the thickness of the film with the number of scanning cycles during deposition. Based in overpotential results, we can conclude that film 5, prepared with 4 mmol L^{-1} $(NH_4)_2[MoS_4]$ at CV during 25 cycles, presented the better electrodeposition conditions for production of MoS_2 film.

The films deposited in optimized conditions were characterized from XRD, SEM, Raman spectroscopy, and optical band gap. XRD analyses were conducted to identify the crystalline structure. In the crystalline MoS_2 material, the presence of three typical diffraction peaks at 14.4, 33.5 and 57.5° corresponded to (002), (101) and (110) planes of MoS_2 (powder diffraction file (PDF) No. 74-932), respectively.[28,29] However, in Figure 3a, it is only possible to observe the diffraction pattern of the FTO substrate (PDF No. 77-451) and an amorphous halo near 20-25°. The absence of characteristic diffraction peaks for crystalline molybdenum sulfide suggested the existence of the amorphous phase, which is consistent with previous reports for films obtained by electrodeposition.[26]

In addition, the SEM presented in Figure 3b shows the globular form, typically obtained for amorphous MoS_2 films, which corroborates with the XRD data.[21,30] The result of the UV-Vis transmission is presented in Supplementary

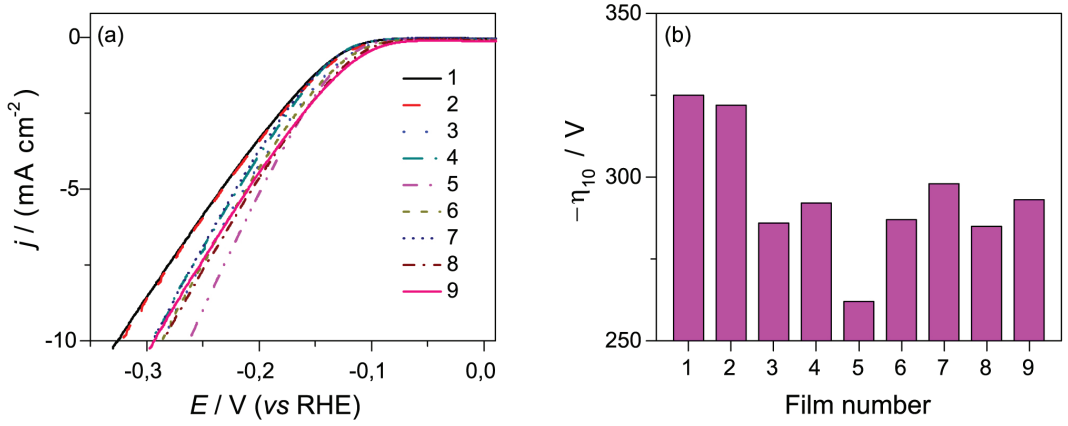

Figure 2. (a) Linear sweep curves in 1.0 mol L^{-1} H_2SO_4 solution at 1 mVs^{-1}; (b) overpotential (-η) at –10 mA cm^{-2} of freshly prepared MoS_2 films on FTO.

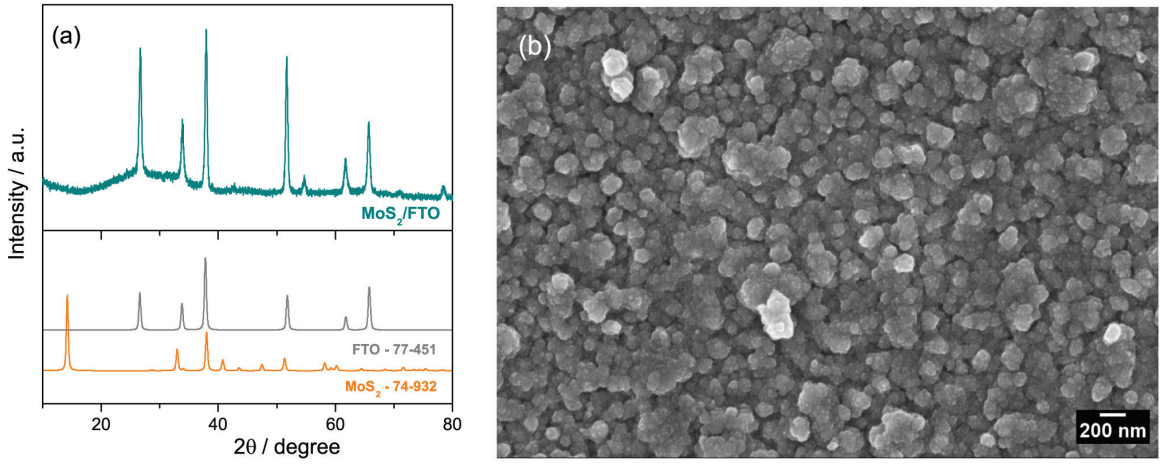

Figure 3. (a) XRD spectra for amorphous molybdenum sulfide film; (b) SEM image of MoS_2 film on FTO (electrode 5, CV deposition, 25 cycles, 4 mmol L^{-1}).

Information (SI) section, Figure S1. A better adjustment of the experimental values was obtained for a value of n = 2, thus reflecting the allowed indirect transition. The value obtained for band-gap energy (Eg) was 1.08 eV, which is in agreement with the value close to 1.1 eV, as presented in the literature.[3]

The Raman spectra of the FTO substrate and the prepared film under the optimized conditions are presented in SI section, Figure S2, in which it is possible to observe the same profile for both samples. Raman spectra revealed the absence of the characteristic peaks expected for crystalline MoS_2, which suggests that crystalline MoS_2 is not present in significant quantities in the as-deposited catalyst and an amorphous MoS_2 film was deposited.

Effect of the Ti substrate on MoS_2 deposition

To analyze the effect of the substrate, we prepared another film on the Ti. It was prepared by cyclic voltammetry at 50 mV s^{-1} between + 0.1 and −1.0 V with 4 mmol L^{-1} of precursor solution during 25 cycles. The profile of deposition is showed in Figure 4. The CV are similar to those observed in FTO substrate with one anodic and one cathodic peaks; therefore, we considered that same process was occurring.

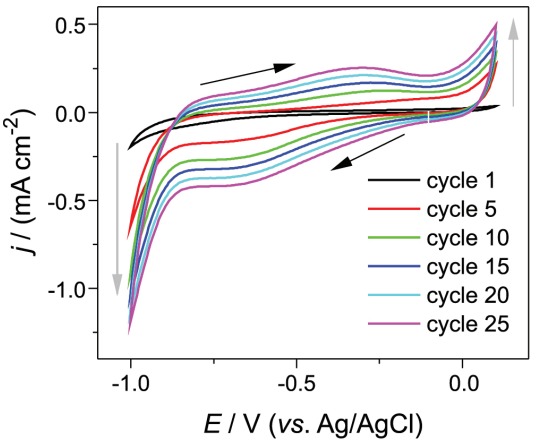

Figure 4. Cyclic voltammetry profile of MoS_2 deposition on Ti substrate in 4 mmol L^{-1} $(NH_4)_2[MoS_4]$ in 0.1 mol L^{-1} $NaClO_4$ at a scan rate of 50 mV s^{-1}.

Figure 5a presents the XRD profiles for MoS_2 films on titanium subtract. There is no evidence of crystalline MoS_2 material, as only the peaks of substrate (Ti, PDF No. 89-3073) were observed. The XRD results were similar to those obtained with the FTO substrate, which suggests

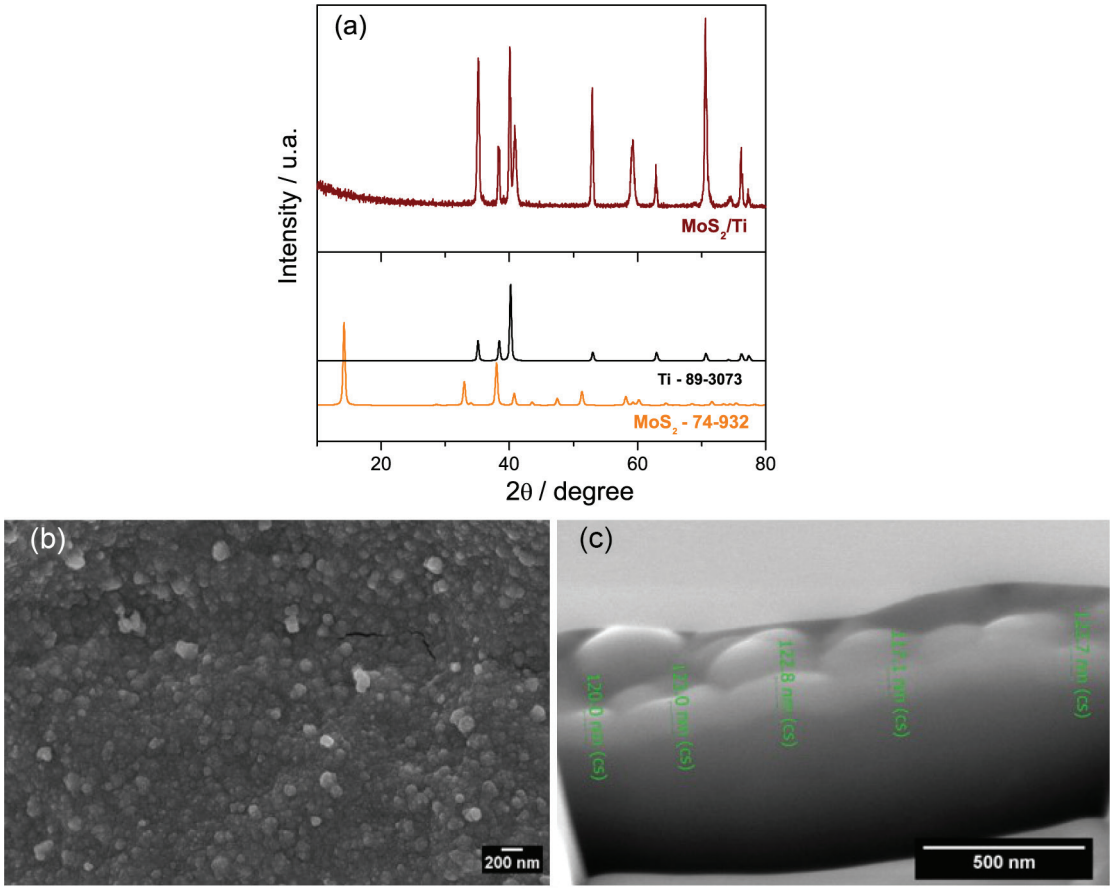

Figure 5. (a) XRD diffraction for amorphous molybdenum sulfide film; (b) SEM image of MoS_2 film on Ti; (c) MoS_2/Ti film thickness. Image obtained by a dual SEM equipped FIB observation equipment.

electrodeposition in MoS_2 in an amorphous phase. The morphology of the film was evaluated by SEM and the image obtained is showed in Figure 5b. As can be seen, the globular form was observed for the Ti/MoS_2 as well as for the FTO/MoS_2 sample.

Figure 5c shows the results of the thickness value for the five regions of MoS_2/Ti film. The resulting film has an average thickness of 121 nm. This result was in agreement with the literature for a MoS_2 film prepared by cyclic voltammetry technique during 50 scan cycles and 4 mmol L^{-1} $(NH_4)_2[MoS_4]$ that presents a thickness between 100 and 137.5 nm.[8]

To observe the distribution of the chemical composition in the film, EDX elemental mapping was carried out for MoS_2/Ti, and the results are presented in Figure 6. In this technique, it is common to realize a deposition of a Pt layer in the region of interest before the cross-sectioning to protect the film from damage. This layer can be seen in the Figure 6a, which was used to perform a mapping of the Ti, Mo, and S elements in the studied area. Mo (Figure 6c) and S (Figure 6d) are homogeneously distributed in the film.

EIS also were performed to evaluate the charge transport in MoS_2 films during the HER. Figure S3 shows the Nyquist plot for MoS_2 film on FTO (Figure S3a) and on Ti (Figure S3b) substrates, in SI. Two semicircles can be seen for both materials, a small on high frequency range (10 kHz-100 Hz) and a large semicircle on lower frequency values. The literature describes the first semicircle to the contact between the substrate and MoS_2 film (R_{film}) and the semicircle at lower frequencies is correlated to charge transfer resistance (R_{ct}) and pseudo-capacitance of (Q_{ct}) charge transfer process.[31,32] For estimated the different resistances, both electrodes samples could be fit with an equivalent electric circuit as showed in Figure S3c, and the values are showed in Table S1 (SI section). R_{film} for FTO was almost 8 times larger than to Ti substrate, indicating that the electrical transport between Ti-MoS_2 is easier than between FTO-MoS_2. In addition, the R_{ct} for Ti was 80% lower than to FTO substrate.

The catalytic activity of the MoS_2/Ti electrode was evaluated by LSV at 1.0 mV s^{-1} in 1.0 mol L^{-1} H_2SO_4, and the polarization curves are shown in Figure 7a. As can be seen in Figure 7a, in Ti bare the current performed to HER. In the presence of MoS_2, the cathodic current started at −0.15 V and increased exponentially due to proton reduction. However, clearly the cathodic current increased faster on MoS_2/Ti, indicating the catalytic effect of this material. The overpotential of −262 and −139 mV was necessary to achieve −10 mA cm^{-2} to FTO/MoS_2 and Ti/MoS_2, respectively. The decrease of 123 mV in the overpotential of HER is very important, because it implies an energy saving for the electrolysis of water.

Tafel analysis is one of the most important methods for evaluating the electrocatalysts for a specific electrocatalytic study of interest, as HER in water electrolysis provides many insights on the kinetic behavior of the electrochemical process. Tafel parameters are Tafel slope (b) and exchange current density (j_o). Tafel slope is related to mechanism of HER at a given electrocatalyst interface, and is usually used to semi-quantitatively predict how much faster the reaction occurs on a given surface. The Tafel plots for the MoS_2/FTO and MoS_2/Ti are shown in Figure 7b.

Volmer-Heyrovsky mechanism is the most common route for a wide range of non-precious metal-based HER catalysts in acidic medium, such as MoS_2. This fact is due to lower availability of electroactive sites on the surface of

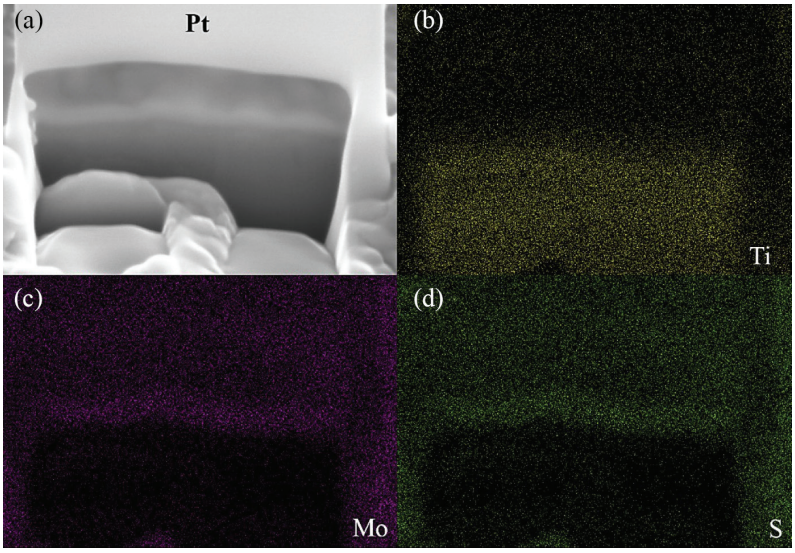

Figure 6. EDX elemental mapping for MoS_2/Ti, with determination of (a) area limiter made by Pt, (b) Ti, (c) Mo, and (d) S.

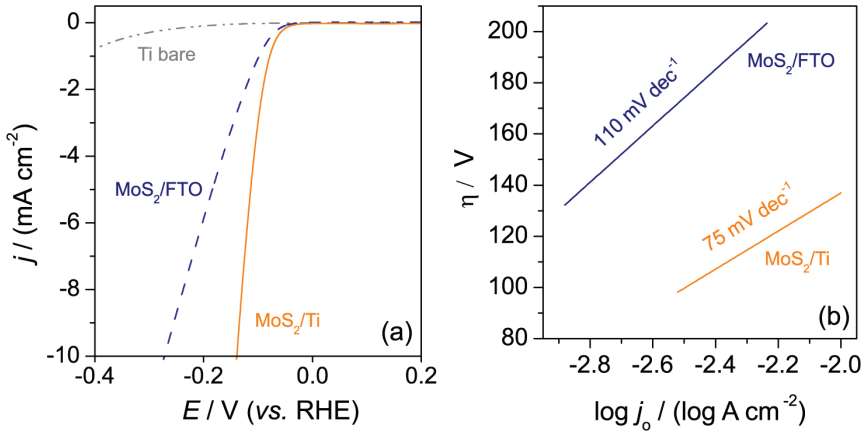

Figure 7. (a) Comparison of polarization curves for different materials in 1.0 mol L^{-1} H_2SO_4 solution at 1 mV s^{-1}; (b) Tafel plot of freshly prepared MoS_2 films on FTO and Ti substrates.

these materials.[25,33] This mechanism involves H adsorption followed of electrochemical discharge of a proton delivery of an H_2 molecule. In these materials the Tafel slopes observed range between 50 to 120 mV dec^{-1}, depending on surface active sites for the reaction. In this work, Tafel slope to MoS_2/Ti and MoS_2/FTO was 75 mV and 110 mV dec^{-1}, respectively, indicating Volmer-Heyrovsky mechanism.[25,33] So on MoS_2/Ti materials deliveries of the H_2 molecules is easier probably due the higher abundance of active sites for the reaction to occur. Also, cconsidering that lower Tafel slope is related with faster the charge transfer across the interface, we can say that Ti favoured the electrocatalytic effect of MoS_2 material. The Tafel results corroborate to the EIS measurement, which showed a lower charge transfer and film resistances for Ti compared to FTO.

For electrochemical active surface area (ECSA) estimation, we associated the non-faradaic capacitive current with the electrochemical double layer charging upon repeated potential cycling in different scan rates. The relationship between the double layer charging current (i_c), the scan rate (v) and the electrochemically active surface area (A_{echem}) can be described as $i = av^b$ in which "a" is the coefficient that corresponds to the pseudo-capacitance value and is directly proportional to the ECSA.[27,34,35]

The average activity of each site can be related with the pseudo-capacitance value, 2 and 4 mF cm^{-2} for the MoS_2/FTO and MoS_2/Ti electrodes, respectively, as shown in Figure S4 (in SI section). In accordance with the Jaramillo and co-workers,[35] these capacitances values correspond to a surface site density of 3.88×10^{16} MoS_2 sites cm^{-2} on FTO and 7.76 MoS_2 sites cm^{-2} on Ti. From these analysis, we can evaluate that MoS_2/Ti presents an increase in the ECSA, comparing with the MoS_2/FTO electrode. We can still estimate the turnover frequency (TOF) *per* surface site, for the MoS_2 film on Ti substrate, which was of 0.4 H_2 s^{-1} at a current density of 10 mA cm^{-2}. This value is consistent with other dates in the literature.[27,34,35]

In addition to catalyst performance studies, j_o was calculated from the inverse of the logarithmic current density at the equilibrium potential of the process in the study. Table 2 presents some values of overpotential at 10 mA cm^{-2} ($-\eta_{10}$), the Tafel slope (b) and exchange

Table 2. HER parameters of MoS_x-based films reported in literature

Material	Synthesis	$-\eta_{10}$ / mV	b / (mV dec^{-1})	j_o / (μA cm^{-2})	Reference
Pt	commercial	10	33	978	30, 36
MoS_2 nanoparticles/Au	drop-casting	ca. 300	69	9.3	37
$MoS_{(2+x)}$/vulcan carbon	chemical reduction	200	35	–	29
MoS_2/C nanospheres	chemical route	207	73	15	30
MoS_x/C nanotube	low-temperature precursor decomposition	200	40	33	15
$MoS_{2x}Se_{2(1-x)}$ nanotube	solvothermal	219	55	–	9,38
MoS_3 and MoS_2 particles	chemical reduction	200	54	–	26
Amorphous MoS_3	chemical reduction	272	53-65	–	35
MoS_x/TiO_2 nanotube arrays	electrodeposition	197	53.3	–	27
MoS_2/FTO	electrodeposition	240	110	83	this work
MoS_2/Ti	electrodeposition	139	75	146	this work

$-\eta_{10}$: overpotential at 10 mA cm^{-2}; b: the Tafel slope; j_o: exchange current density; FTO: fluorine-tin doped oxide.

current density (j_o) for other MoS_2 electrocatalysts from the literature and for our MoS_2/FTO and MoS_2/Ti samples. The resulting value is 146 μA cm^{-2} to Ti substrate. This value is much larger than the most electrodes of MoS_2 studied. Comparing the films produced in this work, j_o increase 75% when FTO is exchanged by Ti. This result is indicative that on Ti substrate the electron transfer rate is very fast, which should be responsible for the high activity of the surface.

Another important parameter to study in electrocatalysis is the stability of the material.[9] We examined this parameter by cycling 1,000 times the electrode between 0.1 and −0.7 V (*vs*. Ag/AgCl) with a scan rate of 100 mV s^{-1} in 1.0 mol L^{-1} H_2SO_4. After this experiment, the electrode was used in another LSV measurement, and the resulting polarization curve was compared with the values obtained from fresh electrodes, as seen in Figure 8. As can be seen, only a slight activity loss in the electrode response was observed at 1,000 cycles. The overpotential in −10 mA cm^{-2} was changed from −139 to −151 mV, and this value presented less than 10%. These results indicate that the MoS_2/Ti electrode has good stability for HER applications in an acidic medium.

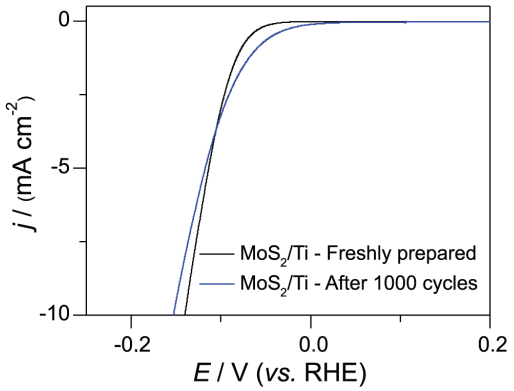

Figure 8. Polarization curves in 1.0 mol L^{-1} H_2SO_4 solution at 1 mV s^{-1} of freshly prepared MoS_2 films on FTO and after 1,000 scanning cycles.

Conclusions

To sum up, we produced an electrode to apply in HER that is inexpensive, easy to fabricate and stable using electrodeposition technique. The best electrodeposition condition was 25 scanning cycles in 4 mmol L^{-1} $(NH_4)_2[MoS_4]$. The films produced was amorphous MoS_2 on Ti substrate. This film presented the low overpotential of −139 mV in −10 mA cm^{-2}. This is the one most positive onset potential that has been reported for amorphous MoS_2 obtained by electrodeposition. The exchange density current, 146 μA cm^{-2}, was 75% higher than MoS_2/FTO prepared in the same way. All results indicated that the Ti substrate promoted a better rate of electron transfer in the catalyst's surface. The MoS_2/Ti sample have shown good stability with the loss of 10% in the overpotential need for HER. Other advantage is that Ti substrate is a good material for use in electrode due to its abundance, low toxicity, high chemical resistance and possibility to apply in photoelectrocatalysis.

Supplementary Information

Supplementary information (Tauc plot, Raman spectra of MoS_2/FTO, EIS spectra and electrochemical capacitance measurements) is available free of charge at http://jbcs.sbq.org.br as a PDF file.

Acknowledgments

The authors thank the São Paulo Research Foundation (FAPESP) for financial assistance to the project and for the fellowships granted (Nos. 2018/16401-8, 2017/12794-2), FAPESP/CDMF (No. 2013/07296-2), and FAPESP/GSK (No. 2014/50249-8). The authors also wish to thank to the Coordination for the Improvement of Higher Education Personnel, Brazil (CAPES), finance code 001 and, by Brazilian National Council for Scientific and Technological Development (CNPq, No.167430/2017-3) for fellowships granted.

References

1. Elmer, T.; Worall, M.; Wu, S. Y.; Riffat, S. B.; *Renewable Sustainable Energy Rev.* **2015**, *42*, 913.
2. Badwal, S. P. S.; Giddey, S.; Kulkarni, A.; Goel, J.; Basu, S.; *Appl. Energy* **2015**, *145*, 80.
3. Gupta, N. M.; *Renewable Sustainable Energy Rev.* **2017**, *71*, 585.
4. Wang, J. Y.; *Energy* **2015**, *80*, 509.
5. Zhang, Q.; Zhong, H.; Meng, F.; Bao, D.; Zhang, X.; Wei, X.; *Nanochem. Res.* **2018**, *11*, 1294.
6. Minggu, L. J.; Wan Daud, W. R.; Kassim, M. B.; *Int. J. Hydrogen Energy* **2010**, *35*, 5233.
7. Benck, J. D.; Hellstern, T. R.; Kibsgaard, J.; Chakthranont, P.; Jaramillo, T. F.; *ACS Catal.* **2014**, *4,* 3957.
8. Zhong, H. X.; Zhang, Q.; Wang, J.; Zhang, X. B.; Wei, X. L.; Wu, Z. J.; Li, K.; Meng, F. L.; Bao, D.; Yan, J. M.; *ACS Catal.* **2018**, *8*, 3965.
9. Liu, K.-H.; Zhong, H.-X.; Li, S.-J.; Duan, Y.-X.; Shi, M.-M.; Zhang, X.-B.; Yan, J.-M.; Jiang, Q.; *Prog. Mater. Sci.* **2018**, *92*, 64.
10. Liu, K.; Zhong, H.; Meng, F.; Zhang, X.; Yan, J.; Jiang, Q.; *Mater. Chem. Front.* **2017**, *1*, 2155.

11. Zhong, H.-X.; Wang, J.; Zhang, Q.; Meng, F.; Bao, D.; Liu, T.; Yang, X.-Y.; Chang, Z.-W.; Yan, J.-M.; Zhang, X.-B.; *Adv. Sustainable Syst.* **2017**, *1*, 1700020.
12. Wang, J.; Zhong, H.-X.; Wang, Z.-L.; Meng, F.-L.; Zhang, X.-B.; *ACS Nano* **2016**, *10*, 2342.
13. Wang, Z.-L.; Hao, X.-F.; Jiang, Z.; Sun, X.-P.; Xu, D.; Wang, J.; Zhong, H.-X.; Meng, F.-L.; Zhang, X.-B.; *J. Am. Chem. Soc.* **2015**, *137*, 15070.
14. Merki, D.; Fierro, S.; Vrubel, H.; Hu, X.; *Chem. Sci.* **2011**, *2*, 1262.
15. Li, D. J.; Maiti, U. N.; Lim, J.; Choi, D. S.; Lee, W. J.; Oh, Y.; Lee, G. Y.; Kim, S. O.; *Nano Lett.* **2014**, *14*, 1228.
16. Li, H.; Tsai, C.; Koh, A. L.; Cai, L. L.; Contryman, A. W.; Fragapane, A. H.; Zhao, J. H.; Han, H. S.; Manoharan, H. C.; Abild-Pedersen, F.; Norskov, J. K.; Zheng, X. L.; *Nat. Mater.* **2016**, *15*, 48.
17. Merki, D.; Hu, X. L.; *Energy Environ. Sci.* **2011**, *4*, 3878.
18. Tributsch, H.; Bennett, J. C.; *J. Electroanal. Chem.* **1977**, *81*, 97.
19. Pham, K. C.; Chang, Y. H.; McPhail, D. S.; Mattevi, C.; Wee, A. T. S.; Chua, D. H. C.; *ACS Appl. Mater. Interfaces* **2016**, *8*, 5961.
20. Morales-Guio, C. G.; Hu, X. L.; *Acc. Chem. Res.* **2014**, *47*, 2671.
21. Lee, S. C.; Benck, J. D.; Tsai, C.; Park, J.; Koh, A. L.; Abild-Pedersen, F.; Jaramillo, T. F.; Sinclair, R.; *ACS Nano* **2016**, *10*, 624.
22. Laursen, A. B.; Kegnaes, S.; Dahl, S.; Chorkendorff, I.; *Energy Environ. Sci.* **2012**, *5*, 5577.
23. Laursen, A. B.; Vesborg, P. C. K.; Chorkendorff, I.; *Chem. Commun.* **2013**, *49*, 4965.
24. Vrubel, H.; Hu, X.; *ACS Catal.* **2013**, *3*, 2002.
25. Anantharaj, S.; Ede, S. R.; Karthick, K.; Sankar, S. S.; Sangeetha, K.; Karthik, P. E.; Kundu, S.; *Energy Environ. Sci.* **2018**, *11*, 744.
26. Vrubel, H.; Merki, D.; Hu, X.; *Energy Environ. Sci.* **2012**, *5*, 6136.
27. Yang, P.; Wang, B.; Liu, Z. Q.; *Int. J. Hydrogen Energy* **2018**, *43*, 23109.
28. Zhang, T.; Zhang, H.; Ji, Y.; Chi, N.; Cong, Y.; *Electrochim. Acta* **2018**, *285*, 230.
29. Tang, C. Y.; Wang, W.; Sun, A. K.; Qi, C. K.; Zhang, D. Z.; Wu, Z. Z.; Wang, D. Z.; *ACS Catal.* **2015**, *5*, 6956.
30. Sun, H.; Ji, X.; Qiu, Y.; Zhang, Y.; Ma, Z.; Gao, G.-g.; Hu, P.; *J. Alloys Compd.* **2019**, *777*, 514.
31. Vrubel, H.; Moehl, T.; Gratzel, M.; Hu, X. L.; *Chem. Commun.* **2013**, *49,* 8985.
32. Upadhyay, K. K.; Nguyen, T.; Silva, T. M.; Carmezim, M. J.; Montemor, M. F.; *Mater. Chem. Phys.* **2018**, *216*, 413.
33. Shi, Y. M.; Zhang, B.; *Chem. Soc. Rev*. **2016**, *45*, 1781.
34. Pham, K.-C.; Chang, Y.-H.; McPhail, D. S.; Mattevi, C.; Wee, A. T. S.; Chua, D. H. C.; *ACS Appl. Mater. Interfaces* **2016**, *8*, 5961.
35. Benck, J. D.; Chen, Z.; Kuritzky, L. Y.; Forman, A. J.; Jaramillo, T. F.; *ACS Catal.* **2012**, *2*, 1916.
36. Ren, W.; Zang, W.; Zhang, H.; Bian, J.; Chen, Z.; Guan, C.; Cheng, C.; *Carbon* **2019**, *142*, 206.
37. Wang, T. Y.; Liu, L.; Zhu, Z. W.; Papakonstantinou, P.; Hu, J. B.; Liu, H. Y.; Li, M. X.; *Energy Environ. Sci.* **2013**, *6*, 625.
38. Zhang, J.; Wu, M.-H.; Shi, Z.-T.; Jiang, M.; Jian, W.-J.; Xiao, Z.; Li, J.; Lee, C.-S.; Xu, J.; *Small* **2016**, *12*, 4379.

Submitted: February 14, 2019
Published online: May 24, 2019